Cube, Cube-octahedron or Rhombododecahedron as Bases for 3-D shape Descriptions

J. SERRA
Centre de Morphologie Mathématique - Ecole des Mines de Paris
35, rue Saint-Honoré - 77300 Fontainebleau (FRANCE)

December 1, 1998

Abstract

The digital three dimensional objects are usually generated on cubic grids, or in case of anisotropy, on rectangular parallelepiped ones (e.g. stack of sections, confocal microscopy, N.M.R., etc.). In the following it is assumed that, after possible pre-treatment, the data are cubic. Then three digital spheres may be chosen, namely cubes, cube-octahedra or rhombododecahedra. They do not share the same advantages.The cube seems to be more natural. However, the cube-octahedron grid exhibits unit edges of a unique length. Moreover, the size of the elementary ball being smaller (13 pixels, versus 27 for the cube), the computations which involve a range of the successive sizes (i.e. distance function, skeleton, ultimate erosion) are treated more finely. Concerning anisotropies now, the best approach is that based on the rhombododecahedron. First, because this polyhedron is obtained by Minkowski addition of the four diagonals of the cube, which can be considered individually (e.g. chord distribution); second, because its twelve faces are identical. Finally, since th rhombododecahedra partition the space, digital change in resolution can be performed. These comparative properties are illustrated on an example of isolated objects (biological cells) and another of texture(expended polymer), by means of an implementation on standard microcomputer.

1 Introduction

In image processing, 3-D treatments appeared during the 80's for both analysis and synthesis purposes. In the present paper, we concentrate on analysis of images, or more precisely, of stacks of binary images. These piles of sections are nowadays currently produced macroscopically (e.g. NMR), or at microscopical scales (e.g. confocal microscopes). They produce experimental data on 3-D rasters which tend to be cubic. Downstream, these computerized data are

binarized by some techniques we will not consider here. These binary data constitute, by definition, sets in $\mathbb{Z}^3$, as well as estimations of sets of $\mathbb{R}^3$. How to access them? How to extend to the 3-D space the usual 2-D notions of sizes, directions, distances, connectivity, homotopy, etc.? This is what we would like to develop hereafter. What follows is basically a tutorial; however the space graph approach for homotopy and decomposition of cube-octahedra are new results (as far as I know). A survey of literature shows that in 3D morphology, the two places that have been producing the most substantial series of results, and for a long time, are the pattern recognition section, at Delft University of Technology (see in particular P.W. Verbeek [1][2], J.C. Mullikin [3], Jonker [4]) and the Centre de Morphologie Mathématique, at the Ecole des Mines de Paris (see in particular Serra [5], Meyer [6] [7], Gratin [8], Gesbert et al. [9]).

2 Three dimensional grids

By grid, we do not only mean a regular distribution of points in the the 3-D space, but also a definition of the elementary edges, faces, and polyhedra associated with these points. The three crystallographic grids we find below derive from the cube, and are constructed as follows

i/ cubic grid, which is generated by translations of a unit cube made of 8 vertices;

ii/ the centred cubic grid (cc grid) where the centres of the cubes are added to the vertices of the previous grid;

iii/ the face-centred cubic grid (fcc grid) where the centres of the faces are added to the vertices of the cubic grid.

A comprehensive comparison of these grids can be found in F. Meyer's study [6].

2.1 Interplane distances

In the last two grids, the vertices generate square grids in the horizontal planes, and in vertical projection the vertices of plane No n occupy the centres of the squares in plane No $n-1$. We shall say that these horizontal plane are *staggered*. If a stands for the spacing between voxels in the horizontal planes, then the interplane vertical spacing is equal to $a/2$ in the cc case, and to $a\sqrt{2}/2$ in the fcc one.

2.2 First neighbors

Every vertex has

- 6 first neighbors in the cubic case
- 8 first neighbors in the cc case
- 12 first neighbors in the fcc case

Geometrically speaking, when point x is located at the centre of the $3 \times 3 \times 3$ cube, its projections

- on the faces of the cube provide the cubic neighbors
- on the vertices the cc-neighbors
- and on the edges the fcc-neighbors

Fig. (1) illustrates this point. One can see, also, that the first neighbors generate the smallest isotropic centred polyhedron of the grid, i.e. a 7-voxel tetrahedron (cubic case) a 9-voxel cube (cc-grid) a 13-voxel cube-octahedron (fcc grid). Denote them by the generic symbol B, and the n^{th} iteration of B by B_n, i.e.

$$B_n = B \oplus B \quad ... \quad \oplus B \qquad n \text{ times} ,$$

with $B_0 =$ Identity. From the implication $n \geq p \Rightarrow B_n \geq B_p$ $\quad n,p$ non negative integers, from the equality $B_n B_p = B_{n+p}$, and from the symmetry of B we draw (proposition 2.4 in Serra [10]) that the 3-D raster of points turns out to be a metric space (in three different ways, according to the grid), where the smallest isotropic centred polyhedron is the unit ball.

3 Elementary edges, faces, and polyhedra

In order to complete the definition of the grids, we will introduce now elementary edges, faces and polyhedra. Edges are necessary to define paths, hence connectivity. Faces and polyhedra are required to introduce notions such as Euler-Poincare number for example, or more generally, to introduce the graph approach.

3.1 Cubic grid

As elementary edges, the best candidates are obviously the closest neighbors (in the Euclidean sense), i.e. those of fig. (1). However, they are not so numerous, in the cubic and in the cc case, in particular, which leads to poor connections. For example, in the cubic grid, the extremities of the various diagonals are not connected, we meet here a circumstance similar to that which led to the 8 and 4-connectivities in the 2-D grid. For the same reason, the authors who focused on the cubic grid, such as A. Rosenfeld [11], [12] or K.S. Fu [13], at the beginning of the 80's, introduced the 26- and the 6-connectivity on the cubic grid. When the foreground X is 26-connected, then the background X^c is 6-connected and vice-versa. In other words, a voxel $x \in X$ admits, as edge partners, all those voxels $y \in X$ that pertain to the cube $C : 3 \times 3 \times 3$ centred at x. Coming back to fig. (1b), we now have to take into account not only the centres of the cube faces, but also the 12 middle points of its edges, and its 8 vertices. Such an extension

of the connectivity for X is possible only when the connectivity on X^c remains restricted to the six closest neighbors. If not, we should run the risk of over crossings of diagonals of $1's$ and of $0's$, so the faces should be undefined.This dissymmetrical connectivity brings into play a second digital metric, where cube $3 \times 3 \times 3$ is the unit ball. In particular, the boundary of set X^c is

$$\delta X^c = X^c \setminus X^c \ominus C$$

whereas the boundary of set X is defined via the unit tetrahedra T:

$$\delta X = X \setminus X \ominus C$$

We draw from this last equation that $\delta X \ominus T = \emptyset$, and from the previous one that $\delta X^c \ominus C = \emptyset$. The boundary of X is thinner, but it may comprise zones of a thickness 2, and of course lines or fine tubes.

Note also that, unlike tetrahedron T, cube C admits a Steiner decomposition into three orthogonal segments of three voxels length each. Consequently, the dilation $X \oplus nC$ is obtained as the product of three linear dilations of size $2n$ in the three directions of the grid.

3.2 cc grid

The cc grid call very similar comments, but now with staggered horizontal planes. The low number of the first neighbors (i.e. 8) of each voxel suggests to add the second neighbors, in number of six (see fig.1). This results in the unit rhombododecahedron R shown in fig. (2), which exhibits 15 vertices (including the centre), 12 rhomb faces, identical up to a rotation, and 24 edges whose common length is the first neighbor distance.

Just as previously, with the cubic grid, the adjunction of 2nd neighbors complicate the situation, for they cannot be added simultaneously to the $1's$ and $0's$. This results in a 14-connectivity for the grains versus a 8-connectivity for the pores. By comparison with the cubic case, the connectivity contrast between foreground and background is reduced, but it remains.

Again, as previously, a new metric is provided, namely that of the rhombododecahedron. In this metric, the isotropic dilations can be decomposed into segment dilations, since R admits a Steiner decomposition into the four diagonals of the cube $(2, 2, 2)$, i.e.

$$R = \begin{pmatrix} 1 & . \\ . & 0 \end{pmatrix} \oplus \begin{pmatrix} 0 & . \\ . & 1 \end{pmatrix} \oplus \begin{pmatrix} . & -1 \\ 0 & . \end{pmatrix} \oplus \begin{pmatrix} . & 0 \\ -1 & . \end{pmatrix} \qquad (1)$$

where -1, 0, 1 indicate the level of the plane, and where the origin is always assigned to the point of plane 0 [10].

3.3 fcc grid

With the fcc grid, things become simpler [6][8]. We still are in a grid where the odd horizontal planes have been shifted by $(a/2, a/2, 0)$ from the cubic spacing,

but now each voxel x admits 14 nearest neighbors, at a distance $a\sqrt{2}/2$. They form the unit cube-octahedron D, of figure (2), centred at point x. Geometrically speaking, such a high number of first neighbors means that the shape of D is a better approximation of the Euclidean sphere, than those of the cube C and the rhombododecahedron R.

As far as connections are concerned, it becomes cumbersome to resort to 2nd neighbors. Therefore there no longer is a risk of diagonal overcrossing. The existence of an edge no longer depends on the phase under study but exclusively on the intersection between grid and sets: two neighbors $1's$ define an edge in set X, two neighbors $0's$ an edge in set X^c.

Finally X and X^c are treated by the same balls D_n, but the latter cannot be decomposed into Minkowski sum of segments, unlike C and R.

3.4 Conclusion

As a conclusion, three reasons argue in favor of the fcc grid, namely

1/ the shape of the cube-octahedron D provides a better approximation of the unit Euclidean sphere, than C or R (isotropic dilations, skeletons, distance functions, etc. will seem more "Euclidean") ;

2/ D is more condensed: 13 points on 3 consecutive planes (D) are more economic than 15 points on 5 planes (R), or 27 on 3 planes. D leads to thinner boundaries, to finer ultimate erosions, etc. and requires less logical tests in its implementation.

3/ In the fcc grid, the connectivity is based on the first neighbors only, which allows a common approach for grains and for pores (in cubic grid, when one decides to attribute *a priori* more than four possible neighbors to the $1's$ than to the $0's$, a rather severe assumption is made, which holds, paradoxically, on the convexity of the *pores*. Most often, both grains and pores exhibit concave and convex portions, and the 26/6-connectivity assumption is just irrelevant).

Facing these advantages, the weakness of the fcc grid is the staggered organization of its successive horizontal planes. However, is it really a drawback? This is the question we will examine now.

4 Directions

In this section, we analyse how the directions, hence the shapes, are modified when embedding the digital 3-D grids into the Euclidean space. First of all a brief (and last) reminder on our three polyhedra is provided.

4.1 Equidistributed directions in $\mathbb{R}^3$ and in $\mathbb{Z}^3$

In $\mathbb{R}^2$, we can subdivide the unit disc in as many equal arcs as we want. In $\mathbb{R}^3$, unfortunately, such nice simplicity vanishes: given an arbitrary integer n, one cannot find in general n equidistributed directions on the unit sphere, i.e. one cannot partition this sphere into n solid angles which would derive

from one another by rotations (a question related to the famous five Platonian polyhedra). Indeed, the 3-D space may be partitioned only into 2, 4, 6, 8, 12 and 20 equal solid angles. The first two partitions are too poor and the last one hardly reachable by small digital polyhedra. The partitions into 6, 8 and 12 angles are those seen from the centre of a cube, an octahedron and a rhombododecahedron respectively, whose faces are windows.

A second and less known result is the following. The axes of these 6, 8 and 12 solid angles coincide with the vectors from a voxel to its 6, 8 and 12 first neighbors in the cubic, cc and fcc grids respectively

These results directly extend to digital grids. For example, in the cubic grid, there are three sets of equi-angular directions, namely

i/ the three basic directions of the grid;

ii/ the four directions involved in eq. 1, which are also the edges directions of the rhombododecahedron;

iii/ the six following directions

$$\begin{pmatrix} 0 & 1 \\ . & . \end{pmatrix}; \begin{pmatrix} 0 & -1 \\ . & . \end{pmatrix}; \begin{pmatrix} 0 & . \\ 1 & . \end{pmatrix}; \begin{pmatrix} 0 & . \\ -1 & . \end{pmatrix}; \begin{pmatrix} . & 0 \\ 0 & . \end{pmatrix}; \begin{pmatrix} 0 & . \\ . & 0 \end{pmatrix} \quad (2)$$

which correspond to the edge directions of the cube-octahedron.

Note that the dilation of the first three unit vectors (i) generate the unit cube ($2 \times 2 \times 2$), that of the four ones (ii) produces the rhombododecahedron (cf. eq. 1), and that of the six vectors of (eq. 2) the tetrakaidecahedron (but not the cube-octahedron...). In addition, each of these three Steiner polyhedra generates by translation a partition of the 3-D space $\mathbb{R}^3$ or $\mathbb{Z}^3$. The tetrakaidecahedron (fig. 2), a sort of Steiner version of the cube-octahedron, is unfortunately too thick for digital purposes (voxels distributed over five successive planes for the unit size).

As for the cube-octahedron itself, if it cannot be obtained by dilating segments, it admits, however, a decomposition into the Minkowski sum of two tetrahedra. For example

$$\begin{matrix} 0 & 1,-1 & 0 \\ 1,-1 & 0 & 1,-1 \\ 0 & 1,-1 & 0 \end{matrix} = \begin{pmatrix} 0 & -1 \\ -1 & 0 \end{pmatrix} \oplus \begin{pmatrix} 0 & +1 \\ +1 & 0 \end{pmatrix} \quad (3)$$

4.2 Digital fcc grids, virtual staggering

How to produce a stack of staggered square grids, or, equivalently, how to produce a digital unit cube-octahedron? An easy way is to favor the diagonal horizontal directions, as in (Eq. 3). The staggering structure is created automatically, since each of the two diagonal subgrid appears, alternatively, in the successive horizontal planes. The negative counterpart is that half of the voxels only are taken into account. For example, the dilation of (Eq. 3) produces neither the central points at levels +1 and -1, nor the middle points of the sides at level zero. We may always add these points, in order to complete the basic cube-octahedron, but then

i/ We increase the elementary size from 13 up to 19 voxels, hence we become less accurate in delineating boundaries, ultimate erosions, skeletons, etc.

ii/ We lose the advantage of a unique type of edges, which governs homotopy and connectedness properties.

iii/ We do not know what to do with the amount of information carried by the non used voxels.

An alternative solution should consist in interpolating one horizontal grid every two planes. This would add a computational step, but above all, it seems "fiddled": how to weight the four horizontal neighbors, versus the two vertical ones? How to display the resulting grid? etc. Therefore, we propose neither to move nor to remove or even modify, any voxel of the cubic initial data, and to consider each even plane, *as it is*, as being staggered. According as the central plane is odd or even, we then obtain one of the two elementary polyhedra of fig. 3.

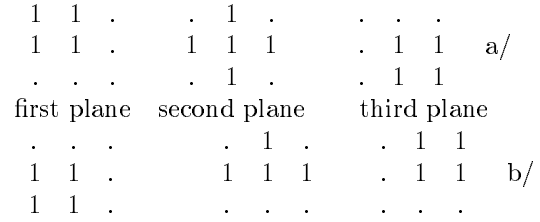

Fig. 3 *: Decomposition of the unit cube-octahedraon in a cubic raster, in order to simulate the staggered structure (a: odd central plane, b: even central plane).*

Such a *virtual staggering* is similar to that used in $\mathbb{Z}^2$, when one generates a hexagonal grid from a square raster. In both cases, the irregularity of the unit polyhedron (resp. polygon) is self-compensated by iteration. In other words, the mappings which bring into play sequences of successive sizes, such as distance functions, medial axes, granulometries, sequential alternated filters, etc. are treated by means of *actual* digital cube-octahedra (resp. hexagons), (see fig. 5).

5 Space graphs and measurements

From now on, we consider sets of points in $\mathbb{Z}^3$, that model the voxels associated with physical objects of the three dimensional space. Sets are given capital letters (X, A, B...), and points small letters.

One find a rather important literature on digital surface description, and calculus, for 3-D sets [2][6][9][11][14][15]. If one has in mind to bridge the gap between digital and continuous spaces, i.e. to provide a Euclidean meaning with digital measurements, the techniques based on digital boundary measurement (i.e. volume difference between dilate and object, or object and eroded set) are not acceptable, and one must deal with stereology [6][9][15][16]. Below we follow

this approach (note that [2] turns out to be an improvement of the classical stereological method). Moreover we are not exclusively interested in surface area, but more generally in digital estimators of "good" Euclidean measurements.

5.1 Reminder on the genus of a surface

The theory of Euclidean surfaces is classical, and dates back to the beginning of the 20th century (R. Poincaré). The comment below derives from [17], more information can be found in general documents such as Encyclopedia Britannica.

In $\mathbb{R}^n$, a *closed orientable surface* is topologically equivalent to a sphere with an even number $2p$ of holes (made by removing discs) which have been connected in pairs by p *handles* (shaped like the surface of half of a doughnut). A *closed non orientable surface* is topologically equivalent to a sphere which has had a certain number q of discs replaced by *cross-caps*. The numbers p and q are said to be the genus of the surface not being closed means that some discs have been removed and the hole left open. A torus is a sphere with one handle; a Möbius strip is a sphere with one cross-cap and one "hole"; a Klein bottle is a sphere with two cross-caps; a cylinder is a sphere with two "holes". In general, the Euler-Poincaré number of a surface is equal to $2 - 2p - q - r$, where p is the number of handles, q is the number of cross-caps (zero for an orientable surface), and r is the number of holes (or boundary curves). The Euler Poincaré number of the union of disjoint surfaces is the sum of each of them.

5.2 Euler-Poincaré number and space graphs

Here, a convenient set model is the class of all finite unions of compact convex sets. This class, called "the convex ring of $\mathbb{R}^n$" allows to elaborate a theory about measurements (Hadwiger theorem below), and on the other hand lends to digitization (space graphs below). In this framework, a deep property of Euler-Poincaré number is stated by the following theorem [18].

Theorem 1 *(Hadwiger): the only functional defined on the convex ring in $\mathbb{R}^n$, of degree zero, invariant under displacements, C-additive and constant for the compact convex sets, is the Euler-Poincaré number ν.*

This topological number ν allows to bridge the gap between Euclidean and digital spaces, since it can be equivalently defined in both modes when we interpret it in terms of graphs. In two dimensions, ν is classically expressed via planar graphs. In $\mathbb{R}^3$, a *space graph* is

i/ a set X of *points* ;

ii/ a collection E of *edges*, i.e. of lines homotopic to the segment [0,1]. Both extremities of each edge belong to X, and two edges may possibly meet at their extremities only ;

iii/ a collection E of faces, i.e. of surfaces homotopic to the closed unit disc. The contours of the faces are exclusively edges, and two faces may possibly intersect along edges only ;

iv) a collections of blocks P, i.e. the connected components of the space that remain when all points, edges and faces of a space graph have been removed.

The space graph is *the* turning point between Euclidean and digital spaces, for the questions investigated here. Defined in $\mathbb{R}^3$, it may also be reinterpreted in $\mathbb{Z}^3$, and the derived relations (e.g. Eq. 4) are meaningful in both spaces.

One proves by induction [5, p. 229], that when set X is finite, or at least locally finite, the Euler-Poincaré constant $\nu(Y)$ set $Y = X \cup E \cup F$ formed by the points, the edges and the faces of X is equal to ( ) :

$$\nu(Y) = N(vertices) + N(faces) - N(edges) - N(blocks) \qquad (4)$$

Seen from a digital point of view, the problem consists now in associating space graphs with the set of points in $\mathbb{Z}^3$. Then, clearly, embedding such graphs in $\mathbb{R}^3$ allows a digital interpretation of their Euler-Poincaré numbers.

Various examples of such "polyhedrizations" are described in literature. The probably oldest one [19] deals with cubic grid and provides an algorithm for $\nu(Y)$ from (Eq 4). According to the choice of connectivities other cubic graph are possible [12][13]. The literature about the rhombododecahedric graphs is undoubtedly more reduced [5][9]. An excellent study on the topological properties of the cubic grid, due to G. Bertrand, will be found in [20]. The last reference also gives a solution to Eq. 4 for the graphs on cc grid. We focus here on the most interesting case, namely the space graphs over fcc grid.

In the fcc case, the graph edges associated with a set X are the pairs of neighboring points of X, the faces are the elementary triangles generated by three (two by two) neighbors, and the blocks are the resulting tetrahedra and octahedra. Unlike the triangles, the elementary squares do not constitute faces in the graph structure, and, for this reason, the elementary pyramids are no longer blocks. Finally, all these definitions are also valid, by duality, to X^c, i.e. to the set of 0's

When applied to a cfc graph X, relation (Eq. 4) reduces to the six configurations drawn in fig. 4.

Note that unlike the number of particles, number ν is a local *measurement* : one needs only small neighborhoods around best points to estimate it statistically.

5.3 Minkowski measures

Euler-Poincaré number, that we have just introduced in the three-dimensional cases, is indeed defined by induction in any $\mathbb{R}^k$. In particular :

- for $k = 0$, the space is reduced to one point and $\nu_0(X) = 1$ iff X is this point ;

- for $k = 1$, $\nu_1(X)$ equals the number of segments of X ;

- for $k = 2$, $\nu_2(X)$ equals the number of particles of X minus their holes.

Consider now a 3-D Euclidean set X, and a subspace $S(x, \omega)$ of location x and orientation ω. Take the cross section $X \cap S(x, \omega)$ and integrate its ν_k-constant over the displacements, i.e. in x and in ω. According to Hadwiger's

theorem, we then obtain the only functionals to be invariant under displacements, c-additive, homogeneous of degree $n-k$, and continuous for the compact convex sets, namely (up to a multiplicative constant) :

$$\begin{array}{lllll} \textit{volume} & v(X) & = & \int_{\mathbb{R}^3} \nu_0\left(X \cap \{x\}\right)\ dx & (5) \\ \textit{surface area} & \frac{1}{4}s(X) & = & \frac{1}{4\pi}\int_{4\pi} d\omega \int_{\pi\omega} \nu_1\left[X \cap \Delta\left(x,\omega\right)\right]\ dx & (6) \\ \textit{mean caliper} & d(X) & = & \frac{1}{4\pi}d\omega \int_{4\pi} d\omega \int_{-\infty}^{+\infty} \nu_2\left[X \cap \Pi\left(x,\omega\right)\right]\ dx & (7) \end{array}$$

At first glance, the notation seems heavy ; in fact, it is extremely meaningful. In (Eq. 6) for example, ω indicates a direction on the unit sphere, and $\Delta\left(x,\omega\right)$ a test line of direction ω passing through point x. The first sum integrates over a plane Π_ω, orthogonal as ω, as the foot x of $\Delta\left(x,\omega\right)$ spans Π_ω. The second integral, in $d\omega$ is nothing but a rotation averaging (similar comment for Eq 7). The meaning of these relations is clearly stereological. For example, the surface area, a 3-D concept, turns out to reduce to a sum of number of intercepts, i.e. a typically 1-D notion.

When set X admits at each point of its surface a mean curvature C and a total curvature C', then mean caliper and Euler-Poincaré number take another geometric interpretation, since

$$2\pi d(X) = \int_{\delta X} C\ ds \qquad \text{and} \qquad 4\pi\nu_3(X) = \int_{\delta X} C'\ ds$$

The three relations (Eq. 5) to (Eq. 7) attribute a *Euclidean* meaning to *digital* data (we meet again the turning point aspect of space graphs). By discretization, (Eq. 5) becomes

$$v*(X) = (\text{Number of voxels of } X) \times v_0$$

where $v_0 = a^3$ (cubic grid) or $a^{3/4}$ (fcc grid) or $a^{3/2}$ (cc grid).
Similarly, (Eq. 6) is written

$$s^*(X) = (\text{average number of intercepts}) \times 2a^2\sqrt{2}$$

where the averaging is taken over the six directions of (Eq. 2), in the cubic grid. Since estimate $s^*(X)$ concerns the Euclidean surface $s(X)$, it differs from the facets areas of the digital set X. For example, here, a facet of a zero thickness counts twice.

5.4 Other measurements

Being stereological is not an exclusive property of Minkowski functionals. Here are two instructive counter examples.

Roughness : Assume that δX admits curvatures everywhere, and let $F(l)$ be the combined chord distribution of X and X^c. Then, near the origin we have [21]

$$F(l) = \frac{l^2}{16}\left[-C' + 3\int_{\delta X} C^2 ds\right]$$

In particular, when X is a physical relief, the term C' vanishes, and the slope of the intercepts density near the origin is proportional to the average of the square mean curvature C^2. It was taken advantage of this descriptor to study road surfaces from profiles.

3-D contacts: Consider a random packing of spheres of radius R, and a cross section through it. The spheres becomes discs, and the distribution of the shortest distances between discs follows a law

$$F(l) \simeq 1.438 \quad n_c(lR)^{1/2}$$

where n_c is the number of contacts between spheres per unit volume [22]. This law, which governs some modes of thermic and electric permeabilities, has been experimentally verified J-P. Jernot.

Both above measurements are invariant under displacement, homogeneous, continuous on convex sets, but, unlike Minkowski functional, do fulfill the c-additivity condition

$$\mu(X \cup X) + \mu(X \cap X') = \mu(X) + \mu(X')$$

which is not essential here.

6 Increasing operations and their residues

As soon as spheres and lines (in a set of directions) are digitally defined, it becomes easy to implement isotropic and linear dilations and erosions, hence openings, closings, granulometries, and all usual morphological filters.

Similarly, the residuals associated with distance function, i.e. skeletons (in the sense of "erosions\openings"), conditional bisectors, and ultimate erosions derive directly.

Examples of fig. 5 illustrate this point.

7 Thinnings, thickenings, and homotopy

After the measurements, the second use of the space graphs concerns thinnings and thickenings, and more particularly, those operators that preserve homotopy.

Given two erosions ε_1 and $\varepsilon_2 : \mathcal{P}(E) \rightarrow (E)$, one defines the hit-or-miss transformation as [5]:

$$X \rightarrow \varepsilon_1(X) \cap \varepsilon_2(X^c) \qquad\qquad X \subset E$$

Then, set X is *thinned* by $(\varepsilon_1, \varepsilon_2)$ when its hit-or-miss transform is subtracted, and it is *thickened* when added. If θ and τ stand for thinning and thickening operators respectively, we have

$$\theta(X) = X \cap [\varepsilon_1(X) \cap \varepsilon_2(X^c)]^c$$
$$\tau(X) = X \cup [\varepsilon_1(X) \cap \varepsilon_2(X^c)]$$

Unlike erosion and dilation, thinning and thickening may satisfy constraints for homotopy preservation. In two dimensions comprehensive studies have been performed on this subject by C. Arcelli and G. Sanniti di Baja, in Naples, for the square grid [see among others 23], and by J. Serra for the hexagonal one [5]. In three dimensions, for the cubic grid the most important achievements are due to the Delft school, namely S. Lobregt et al. [24], and more recently P. Jonker [4]. One may mention also some pioneer work by T. Yf and K.S. Fu [13]. Concerning fcc grid, the results are considerably more limited, however some attempts by P. Bhanu Prasad and P. Jernot [25], and by J.H. Kimberly and K. Preston [26] may be indicated. A general comment on all these 3D analyses, is that each of them proposes a unique algorithm, whose genesis is never explicited and whose justification is provided by one or two examples.

Now, in 3D, just as in 2D, the homotopy of a bounded set X, may be represented as a tree. Starting from the background, one first considers all the connected components δX_i of δX that are adjacent to the background. They form the first level of the tree. With each of them is associated a genus. Some δX_i enclose inside areas. If Y_i is the inside of a δX_i, Y_i may contain in turn boundaries of X, say $\delta Y_{i,j}$; each of them admits a certain genus, etc. The collection of the $\delta Y_{i,j}$ form the branches of the tree that derives from Y_i ; ... and so on.

Two sets are homotopic when their homotopy trees are identical, and a mapping $X \rightarrow \psi(X)$ is homotopic when for all X, $\psi(X)$ is homotopic to X.

From now on, we limit ourselves to the neighborhood mappings. They are not the only ones able to preserve homotopy, but the simplest ones in the translation invariant approach. In such a case, each pixel is compared with a neighborhood, which is always the same modulo a translation, and the pixel is kept or removed according to the configuration of the neighborhood. We find again the thinning operator.

Such thinning will be homotopic when by changing $1 \rightarrow 0$ we do not locally modify the genus of the boundaries. Since it holds on boundary, such a condition is symmetrical for X and X^c ; i.e. the change must not open a hole, neither create a new particle ; must not generate a donut of grains or of pores, neither suppress a grain or a pore, etc. On the fcc grid, the neighborhood of size one around a voxel x admits all the edges involved in the unit cube-octahedron $D(x)$ centred at point x. But since the squares are *not* faces, this neighborhood exhibits six pyramidal hollows, as shown in fig. 6a.

On the unit cube-octahedral sphere $\delta D(x)$ (i.e. $D(x)$ minus its centre x), the only admissible configurations of 1's and 0's are those which result in a simply connected component of 1's, say T_1 and also of 0's, say T_0. One easily verifies that the other ones may change homotopy.

A convenient way to group and classify the admissible configurations consists in taking for $T_1(x)$ one point, these two connected point, and three, etc. of $\delta D(x)$, considering the neighbors of $T_1(x)$ on $\delta D(x)$ as a no man's land, and taking for $T_0(x)$ the remaining voxels of $\delta D(x)$. This technique is right if the obtained T_0 is simply connected (which is always true), and if the neighbors of T_0 on δD coincide with those of T_1 (which is not always true, so we have to

exclude some neighborhoods).

We finally obtain five candidate configurations, up to rotations and complement, where T_1 is successively

- 1 point = H_1
- 2 extremities of one edge = K_1
- 3 consecutive summits of a hexagonal section = L_1
- 3 summits of a triangular face = M_1 (fig. 7)
- 4 summits of an elementary square = N_1 (fig. 7)

Moreover, the above conditions are necessary, but not sufficient. If the four summits of a square on $D(x)$ are 0's, then by changing the centre x of $D(x)$ from 1 to 0 one generates a hole in the pores. Therefore in all cases where such a square may arise one must replace the hollow by the octahedron which fills it, i.e. add some of the supplementary point that change fig. 6a into fig. 6b.

Such a completion is not necessary for the first and last above cases (involving H_1 and N_1), but needed for the three other ones. After having completed correctly the structuring elements, one obtains five pores $H = (H_1, H_0)$, $K = (K_1, K_0)$, $L = (L_1, L_0)$, $M = (M_1, M_0)$ and $N = (N_1, N_0)$. Just as in 2D, one can list the geometrical meaning of the corresponding thinnings.

H: for a simply connected particle, thins it down to one point, and thickens it up to its convex hull; it acts independently on disjoint particles, but in thinning only.

K and L : thin the sets down to lines; L but not K is symmetrical under complementation.

M and N : thin the sets down to sheets ; both are symmetrical for the complement.

Their geometrical interpretations are true up to some pathological configurations (just as in 2D, see [5] p. 396 for ex.), which fortunately rarely occur. The above interpretations are drawn from the consideration of the invariant blocs, faces and edges in each thinning.

It would be long and tedious to develop all the structuring elements involved in each operator. More briefly, we indicate in fig. (7), the two configurations M and N, in a perspective display. For the former, some external 1's and 0's have to be added.

8 References

References

[1] P.W. Verbeek, H.A. Vrooman and L.J. van Vliet, "Low level image processing by max-min filters", *Signal Process.,* vol. 15, pp. 249-258, 1988.

[2] J.C. Mullikin and P.W. Verbeek, "Surface area estimation of digitized planes", *Bioimaging,* vol. 1, pp. 6-16, 1993.

[3] J.C. Mullikin, *Discrete and Continuous Methods for Three Dimensional Image Analysis*, Delft: Univ. Press, 1993.

[4] P.P. Jonker, "Parallel processing in computer vision and collision free path planning of autonomous systems", in *26th ISATA*, 1993.

[5] J. Serra, *Image Analysis and Mathematical Morphology*, London: Acad. Press, 1982.

[6] F. Meyer, "Mathematical Morphology: from two dimensions to three dimensions", *J. of Micr.,* vol. 165, pp. 5-29, 1992.

[7] C. Gratin and F. Meyer, "Mathematical Morphology in three dimensions", *Acta Stereol.* vol. 11, pp. 551-558, 1991.

[8] C. Gratin, *De la représentation des images en traitement morphologique d'images tridimensionnelles,* PhD thesis, Ecole des Mines de Paris, 1993.

[9] S. Gesbert, C.V. Howard, D. Jeulin and F. Meyer, "The use of basic morphological operations for 3D biological image analysis", *Trans. Roy. Microsc. Soc.*, vol. 1, pp. 293-296, 1990.

[10] J. Serra, "Mathematical Morphology for Boolean lattices", in *Image Analysis and Mathematical Morphology*, vol. 2, J. Serra (ed.), London: Acad. Press, 1988.

[11] D.G. Morgenhaler and A. Rosenfeld, "Surfaces in three-dimensional digital images", *Information and Control,* vol. 51, pp. 227-247, 1981.

[12] T. Kong and A. Rosenfeld, "Digital topology: Introduction and survey", *Comp. Vis. Image Proc.*, vol. 48, pp. 357-393, 1984.

[13] Y.F. Tsao and K.S. Fu, "A parallel thinning algorithm for 3-D pictures", *Comp. Graph. Image Proc.*, vol. 17, pp. 315-331, 1981.

[14] J. Mukkerjee and B.N. Chatterji, "Segmentation of three-dimensional surfaces", *Pattern Rec. Letters*, vol. 11, pp. 215-223, 1990.

[15] V.C. Howard and K. Sandau, "Measuring the surface area of a cell by the method of the spatial grid with a CSLM", *J. of Micr.,* vol. 165, pp. 183-188, 1992.

[16] P. Bhanu Prasad, J.P. Jernot, M. Coster, J.L. Chermant, "Analyse morphologique tridimensionnelle des matériaux condensés", *in Proc. PIXIM,* 1988, pp. 31-42.

[17] James and James, *Mathematics Dictionary,* Van Nostrand, 1982.

[18] H. Hadwiger, *Vorsesungen über Inhalt, Oberfläche und Isoperimetrie,* Springer, 1957.

[19] J. Serra, "Introduction à la Morphologie Mathématique", *Cahiers du CMM*, Ecole des Mines de Paris, 1969.

[20] G. Bertrand, "Simple points, topological numbers and geodesic neighborhoods in cubic grids", *Pattern Rec. Letters*, vol. 15, pp. 1003-1012, 1994.

[21] J. Serra, "Descriptors of flatness and roughness", *J. of Micr.*, vol. 134, pp. 227-243, 1984.

[22] Y. Pomeau and J. Serra, "Contacts in random packings of spheres", *J. of Micr.*, vol. 138, pp. 179-187, 1985.

[23] C. Arcelli and G. Saniti di Baja, "Width-independent fast thinning algorithms", *IEEE Trans. Pattern Anal. Machine Intell.,* vol. 7, pp. 463-474, 1985.

[24] S. Lobregt, P.W. Verbeek and F.A. Groen, "Three dimensional skeletonization: Principle and algorithm", *IEEE Trans. Pattern Anal. Machine Intell.,* vol. 1, pp. 75-77, 1980.

[25] P. Bhanu Prasad and J.P. Jernot, "Three dimensional homotopic thinning of digitized sets", *Acta Stereol.,* vol. 9, pp. 235-241, 1990.

[26] J.H. Kimberly and K. Preston, "Three dimensional skeletonization on elongated solids", *CVGIP*, vol. 27, pp. 78-91, 1984.